FULL PAPER

Poly(diketopyrrolopyrrole-benzothiadiazole) with Ambipolarity Approaching 100% Equivalency

Shinuk Cho, Junghoon Lee, Minghong Tong, Jung Hwa Seo, and Changduk Yang*

As a characteristic feature of conventional conjugated polymers, it has been generally agreed that conjugated polymers exhibit either high hole transport property (p-type) or high electron transport property (n-type). Although ambipolar properties have been demonstrated from specially designed conjugated polymers, only a few examples have exhibited ambipolar transport properties under limited conditions. Furthermore, there is, as yet, no example with 'equivalent' hole and electron transport properties. We describe the realization of an equivalent ambipolar organic field-effect transistor (FET) by using a single-component visible–near infrared absorbing diketopyrrolopyrrole (DPP)-benzothiadiazole (BTZ) copolymer, namely poly[3,6-dithiene-2-yl-2,5-di(2-decyltetradecyl)-pyrrolo[3,4-c]pyrrole-1,4-dione-5',5''-diyl-*alt*-benzo-2,1,3-thiadiazol-4,7-diyl] (PDTDPP-*alt*-BTZ). PDTDPP-*alt*-BTZ shows not only ideally balanced charge carrier mobilities for both electrons (μ_e = 0.09 cm^2 V^{-1} s^{-1}) and holes (μ_h = 0.1 cm^2 V^{-1} s^{-1}) but also its inverter constructed with the combination of two identical ambipolar FETs exhibits a gain of ~35 that is much higher than usually obtained values for unipolar logic.

1. Introduction

Ambipolar FETs based on conjugated polymers based on both p-type and n-type channels in one device with thereby simplified circuit design and fabrication processes, are particularly attractive for use in low-cost, flexible, and portable electronic applications.[1–3] Since the typical conjugated polymers show either high hole mobility or high electron mobility, scientists have attempted to realize ambipolar FETs by the use of blending systems as an active layer in the channel, or of bilayers separately consisting of hole transporting and electron transporting materials.[4–7] Although ambipolar FETs have been successfully

J. Lee, Prof. C. Yang
Interdisciplinary School of Green Energy
Ulsan National Institute of Science and Technology (UNIST)
100 Banyeon-ri, Eonyang-eup, Ulju-gun, Ulsan, 689-798, Korea
Fax: (+82) 52-217-2909
E-mail: yang@unist.ac.kr
Dr. M. Tong, Dr. J. H. Seo
Center for Polymers and Organic Solids
University of California at Santa Barbara
Santa Barbara, CA 93106-5090, USA
Prof. S. Cho
Department of Physics and EHSRC
University of Ulsan
Ulsan 680-749, South Korea

demonstrated by utilizing these techniques, the achievement of the ambipolarity from a single-component material would be the most ideal strategy due to the attractiveness of easy-solution processing. Thiophene-based conjugated polymers such as poly(3-hexylthiophene) (P3HT) and poly(2,5-bis(3-tetradecylthiophene-2-yl)thieno[3,2-*b*] thiophene) (PBTTT) have been preferred for use as active materials in polymer FETs because of their relatively high mobility.[5,6] The thiophene-based aromatic conjugated polymers, however, generally showed unipolar hole transport because of the electron-rich nature of the thiophene rings. Recently, with the increasing attention on low band gap polymers based on donor (D)–acceptor (A) architecture, electron deficient units (electron acceptor) such as benzothiadiazole (BTZ),[8] benzo[1,2-*c*;4,5-*c*']bis[1,2,5]thiadiazole (BBT),[4] and diketopyrrolopyrrole (DPP)[7,9] have been introduced into the polymer backbones, and are expected to realize effective ambipolar behavior.
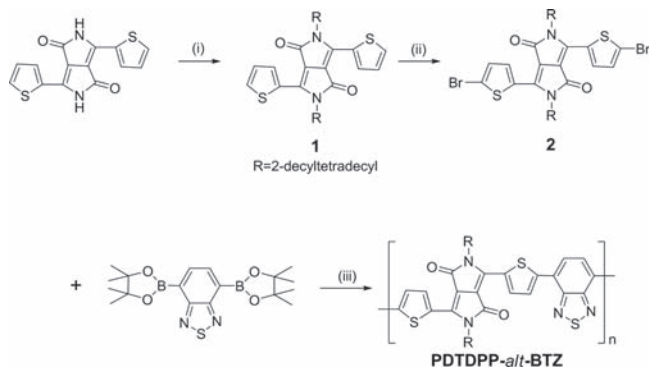
Although Marks and coworkers have demonstrated ambipolar FETs based on the indenofluorenebis(dicyanovinylene) core,[10] the measured mobility was only ~10^{-4} cm^2 V^{-1} s^{-1}; i.e., lower than bulk-heterojunction (BHJ) bipolar FETs. Bürgi et al. reported ambipolar near-infrared light-emitting FETs using poly[3,6-bis-(4'-dodecyl-[2,2']bithiophenyl-5-yl)-2,5-bis-(2-hexyl-decyl)-2,5-dihydro-pyrrolo[3,4-]pyrrole-1,4-dione] (BBTDPP1). Janssen and coworkers reported the 'nearly' balanced ambipolar material, PDPP3T, with alternating diketopyrrolopyrrole (DPP) and terthiophene units.[4,7] However, the hole mobility was higher than the electron mobility. In addition, the threshold voltage of electron channel is higher than threshold voltage of hole channel. To improve electron transport, we introduce one more electron deficient building block, benzothiadiazole (BTZ), in the D–A alternating copolymer consisting of DPP and two unsubstituted thiophene rings, namely poly[3,6-dithiene-2-yl-2,5-di(2-decyltetradecyl)-pyrrolo[3,4-*c*]pyrrole-1,4-dione-5',5''-diyl-*alt*-benzo-2,1,3-thiadiazol-4,7-diyl] (PDTDPP-*alt*-BTZ). Recently, the initial results on ambipolar PDTDPP-*alt*-BTZ FETs were reported;[11] here, we investigate thoroughly their optoelectronic features to gain a better understanding and with a view to optimization for high-end applications. We report on the optoelectronic features of PDTDPP-*alt*-BTZ using ultraviolet photoelectron spectroscopy (UPS) that enables determination of the HOMO and LUMO energies, ambipolar FET characteristics,

www.MaterialsViews.com

ADVANCED
FUNCTIONAL
MATERIALS
www.afm-journal.de

FULL PAPER

Scheme 1. Synthetic route to PDTDPP-*alt*-BTZ. Reagents and conditions: (i) 2-Decyltetradecylbromide, K$_2$CO$_3$, DMF, 120 °C, under Ar, 24 h, 55%; (ii) NBS, CHCl$_3$, RT, dark and under Ar, 24 h, 53%; (iii) Pd(pph$_3$)$_4$, K$_2$CO$_3$, toluene/H$_2$O, 95 °C for 72 h, 75%.

density functional calculations of the electronic structure, absorption and ultrafast photoinduced absorption. In addition, we demonstrate a high gain inverter using n-channel and p-channel FETs fabricated from this ambipolar semiconducting polymer.

2. Results and Discussion

The synthesis of PDTDPP-*alt*-BTZ was carried out as depicted in **Scheme 1**. Firstly, 3,6-dithiophen-2-yl-2,5-dihydropyrrolo[3,4-*c*]pyrrole-1,4-dione (DTDPP, **1**) was synthesized according to the procedure in the literature.[12] To improve the solubility and the film-forming ability of DTDPP-based copolymers, two extended 2-decyltetradecyl chains[13] were introduced at the 2,5-positions (N atoms in the lactam ring) of the DTDPP moiety. Dibromination of **1** in CHCl$_3$ afforded 3,6-di(2-bromothiene-5-yl)-2,5-di(2-decyltetradecyl)-pyrrolo[3,4-*c*]pyrrole-1,4-dione (**2**). The alternating copolymer poly[3,6-dithiene-2-yl-2,5-di(2-decyltetradecyl)-pyrrolo[3,4-*c*]pyrrole-1,4-dione-5′,5″-diyl-*alt*-benzo-2,1,3-thiadiazol-4,7-diyl] (PDTDPP-*alt*-BTZ) was synthesized by Suzuki polycondensation in toluene using Pd(PPh$_3$)$_4$ as catalyst, from the dibromo-monomer **2** and commercially available 4,7-diboronicester-2,1,3-benzothiadiazole further purified by recrystallization from methanol. Through a combination of the high purity of two monomers and the compensation for the expected loss in solubility by using the branched solubilizing groups, PDTDPP-*alt*-BTZ can be accessed in high molecular weight, which is a crucial factor for its electronic performance. PDTDPP-*alt*-BTZ has good solubility in common organic solvents such as chloroform, toluene, and chlorobenzene. Molecular weight and polydispersity index (PDI) of PDTDPP-*alt*-BTZ are determined by gel permeation chromatography (GPC) analysis with a polystyrene standard calibration. PDTDPP-*alt*-BTZ has a high number-average molecular weight (M_n) of 135.6 kg mol^{-1} with a PDI of 4.26.

The UV–vis–NIR absorption of PDTDPP-*alt*-BTZ was investigated in chloroform solution and in the films, as depicted in **Figure 1**a. Transparent and uniform polymer film was prepared on quartz by spin-casting from chloroform solution
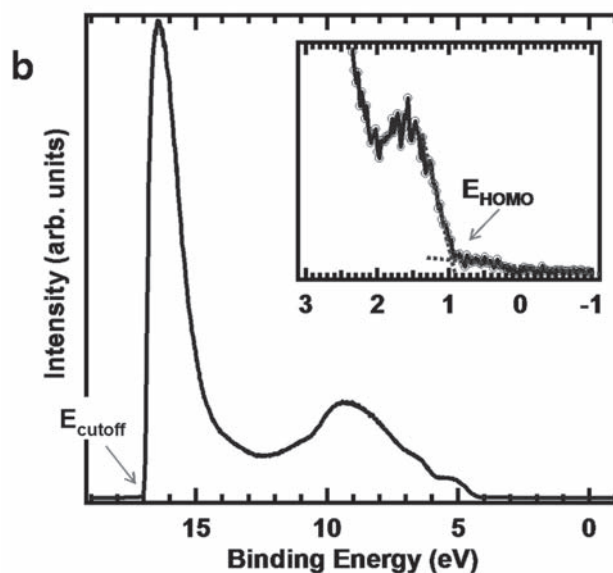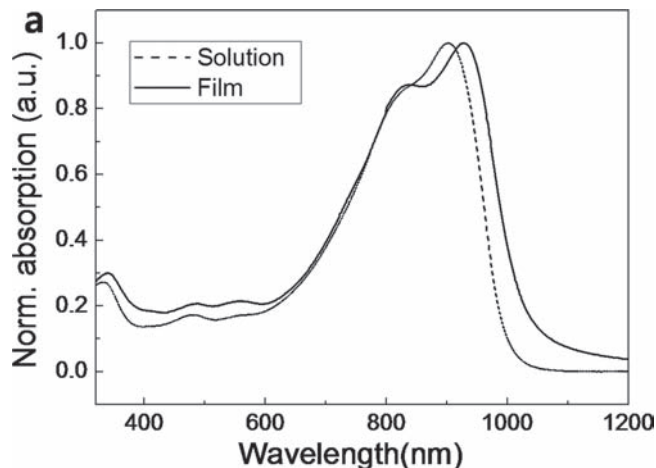

Figure 1. a) UV–vis–NIR absorption spectra of PDTDPP-*alt*-BTZ in dilute CHCl$_3$ solution and thin film on quartz plate. b) UPS spectrum of PDTDPP-*alt*-BTZ.

at room temperature. PDTDPP-*alt*-BTZ in solution displays a strong broad absorption band with a maximum 901 nm covering from 600 to 1000 nm, arising from π–π* transitions in the polymer backbone. Despite that, the profile in shape of absorption spectra of PDTDPP-*alt*-BTZ is essentially unchanged from the solution state to the solid state, the absorption maximum of PDTDPP-*alt*-BTZ in film shows a red-shift by 40 nm compared with that in solution, which is related not only to the intermolecular interaction in the solid state caused by the strong polarity of the lactam groups on DTDPP units[14] but also to the increased vibronic coupling associated with molecular rigidity imposed by molecular connectivity in solution measurement.

Figure 1b displays the ultraviolet photoelectron spectroscopy (UPS) spectrum taken for a PDTDPP-*alt*-BTZ film. The abscissa is the binding energy relative to the Fermi energy (E_F) of Au, which is defined by the energy of the electron before excitation relative to the vacuum level. E_{cutoff} is the high binding

energy cutoff of the PDTDPP-*alt*-BTZ and is determined by linear extrapolation to zero at the yield of secondary electrons.[15,16] Inset of Figure 1b shows the HOMO region. The E_{HOMO} is the onset relative to the E_F of Au (at 0 eV). From Figure 1b, E_{cutoff} is 16.97 eV, and E_{HOMO} is 0.87 eV. The ionization potential (IP, HOMO) is determined by using the incident photon energy (hν = 21.2 eV) for He I, E_{cutoff}, and E_{HOMO} according to the equation,[17,18]

$$IP = h_\nu - (E_{cutoff} - E_{HOMO})$$

The electron affinity (EA, LUMO) is estimated by using the HOMO and the optical gap from the UV–vis–NIR absorption in Figure 1a. The uncertainty of the EA is due to a difference between the true gap and optical gap by the exciton binding energy.[15–19] From the UPS and absorption spectra, the IP and EA of the PDTDPP-*alt*-BTZ are 5.1 eV and 3.9 eV, respectively. Note that the IP of the polymer is about 5.1 eV, which is approximately 0.3 eV greater than that of regioregular P3HT. This suggests that the higher IP arises mainly from the reduced delocalization from the fused DPP aromatic ring. The optical data including the absorption peak wavelength (λ_{max}) in both solution and film, and the optical band gap (E_g^{opt}) as well as the IP value are summarized in **Table 1**.

Figure 2 shows tapping mode atomic force microscopy (AFM) images of PDTDPP-*alt*-BTZ on PPcB modified silicon wafer substrate. These AFM images of PDTDPP-*alt*-BTZ show that they have aggregated granular surfaces. The RMS roughness value is 1.15 nm for a 2 μm × 2 μm scan area. The molecular packing of the copolymer in thin films cast from

Figure 3. a) Schematic device structures of PDTDPP-*alt*-BTZ FET. b) Output characteristics of ambipolar PDTDPP-*alt*-BTZ FET. c) Transfer characteristics of ambipolar PDTDPP-*alt*-BTZ FET under p-type operation (V_{ds}, V_{gs} < 0) and n-type operation (V_{ds}, V_{gs} > 0). d) Transfer characteristics of fully optimized ambipolar PDTDPP-*alt*-BTZ FET fabricated with two different electrodes. Au was used as a source metal and Al was used as a drain metal for easy injection of hole and electron, respectively.

Table 1. Photophysical properties of the copolymer.

PDTDPP-*alt*-BTZ	λ_{max} [nm]		IP [eV]a)	E_g^{opt} [eV]b)
	solution	film		
	901	927	5.1	1.2

a)Determined by ambient ultraviolet photoelectron spectroscopy (UPS) technique;
b)Calculated from the absorption band edge of the copolymer film, $E_g^{opt} = 1240/\lambda_{edge}$

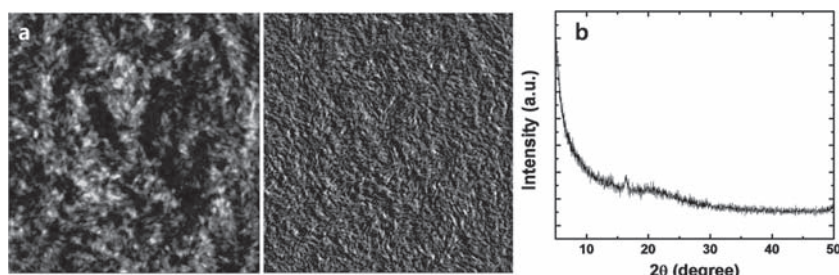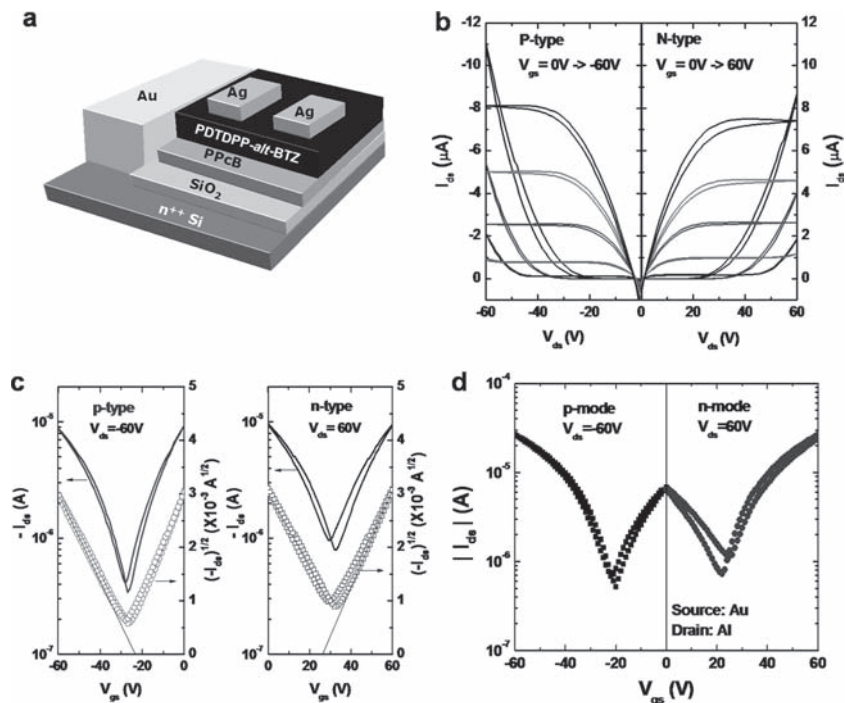**Figure 2.** a) Height (left) and phase (right) AFM images and b) X-ray diffraction (XRD) pattern of PDTDPP-*alt*-BTZ thin film.

solution (onto a Si wafer as substrate) was studied by X-ray diffraction (XRD) analysis. No scattering patterns are observed, suggesting a macroscopically disordered, amorphous solid (Figure 2b).

Figure 3a shows the schematic device structures of PDTDPP-*alt*-BTZ FET fabricated on SiO₂ (200 nm)/n⁺⁺ Si substrate covered by a 60 nm thick layer of spun-cast polypropylene-co-1-butene (PPcB). PPcB layer was introduced as a passivation layer to remove hydroxyl group which acts as trap sites of electrons.[20] Figure 3b shows the output characteristic curves of PDTDPP-*alt*-BTZ FET. Measured output characteristic curves show typical ambipolar characteristics; diode-like curves at low gate bias and saturation curves at high gate bias. Furthermore, it displays beautiful symmetry between p-type operation (V_{ds} < 0, V_{gs} < 0) and n-type operation (V_{ds} > 0, V_{gs} > 0). Figure 3c demonstrates the ambipolar transport properties. PDTDPP-*alt*-BTZ FETs exhibit balanced hole and electron mobilities of 0.061 and 0.054 cm² V⁻¹ s⁻¹, respectively.

We obtained the balanced transport using Ag source-drain electrodes. When different workfunction metals were used as the source and drain electrodes, n-type and p-type performances were systematically changed.[21] For the device with Au electrodes, the hole mobility was slightly higher than the electron mobility. For the FET with Al electrodes, the electron mobility was higher than the hole
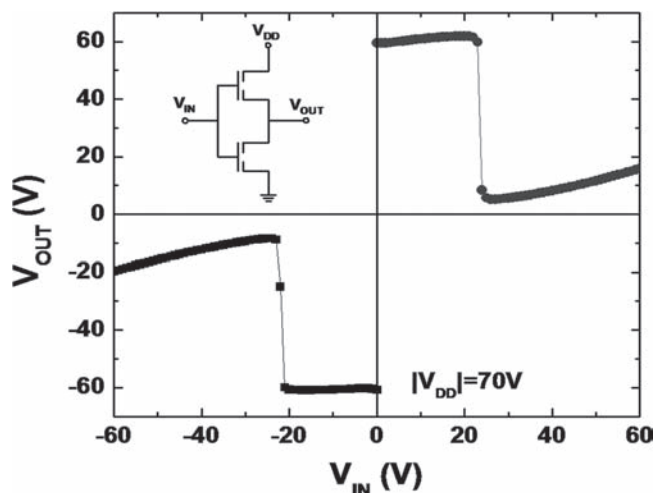
www.MaterialsViews.com

ADVANCED
FUNCTIONAL
MATERIALS
www.afm-journal.de

FULL PAPER

Figure 4. Inverter characteristics of an inverter based on two identical ambipolar PDTDPP-*alt*-BTZ FETs. The steepness of the inverter curve indicates a gain of ~35.

Figure 5. Charge-density isosurface for the HOMO (top) and LUMO (bottom) levels of PDTDPP-*alt*-BTZ. Both HOMO and LUMO isosurface are well delocalized over the entire conjugated main chain.

mobility. Therefore, to obtain maximized hole and electron mobilities, we have made a FET with "two color" electrodes as shown in Figure 2d. The mobilities obtained from the optimized FET with two color electrodes (Au for source electrode and Al for drain electrode) were 0.097 cm^2 V^{-1} s^{-1} for the hole and 0.089 cm^2 V^{-1} s^{-1} for the electron. These values are among the highest ambipolar equivalency reported for single-component polymer ambipolar transistors.

The well balanced ambipolar nature of PDTDPP-*alt*-BTZ FETs prompted us to examine CMOS-like inverters using two identical ambipolar transistors with a common gate as the input voltage (V_{IN}) (see **Figure 4**, inset). Figure 4 shows the output voltage (V_{OUT}) as a function of the input voltage (V_{IN}) at constant supply bias (V_{DD}). The output characteristic of inverter with positive V_{DD} and V_{IN} works in the first quadrant, while the output characteristic of inverter with negative V_{DD} and V_{IN} works in the third quadrant. The steepness of the inverter curve indicated the maximum gain of ~35, which is a relatively good value for single-component-based inverters fabricated from organic FETs.[22–24]

The presence of the ambipolarity is explained by the delocalized character of the HOMO and LUMO on both donor and acceptor regions within the repeat unit of the monomer. **Figure 5** depicts the electron-state-density distribution of the HOMO and LUMO of geometry optimized structures (DFT, B3LYP/6 –31G*) of PDTDPP-*alt*-BTZ (two repeating units) using the Gaussium 03 program. Since the side chains in PDTDPP-*alt*-BTZ do not contribute significantly to the variation of chain conformation and charge-density isosurface, they were excluded from our calculation. The results indicate that the electron density of HOMO and LUMO are delocalized over the entire conjugated monomer (both the acceptor unit and donor unit). Typically, for conventional D–A conjugated copolymers (D–D–A–D structure), electron transport is hindered because of the localized character of the LUMO on the electron-acceptor site.[25] The reason of this localization is that there is no electron wave-function overlap because of relatively long distance
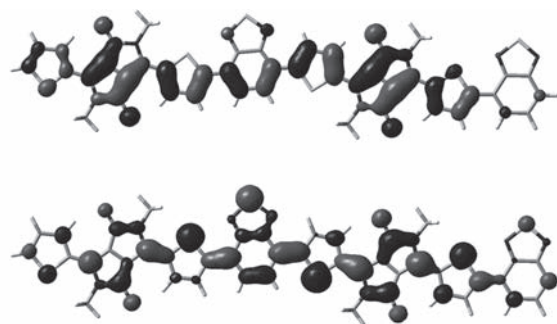
between electron-acceptor sites. However, in the case of our PDTDPP-*alt*-BTZ, since we build D–A–D–A alternating structure, the distance between electron-acceptor sites is shortened with reasonably good overlap of the electron wave-function on successive acceptor sites.

Although the PDTDPP-*alt*-BTZ itself has an ideal band gap as a donor material for BHJ solar cells together with good transport properties for injected charges, no photovoltaic effects are detected in BHJ solar cells fabricated using the blends with PC$_{61}$BM or PC$_{71}$BM.

We found that for pristine PDTDPP-*alt*-BTZ film, the photoresponse is very low and there is no detectable photocurrent in the NIR region (700–1000 nm) in spite of strong absorption as shown in **Figure 6**. This lack of a photoresponse at lower energy peak was also observed on dithienylcyclopentadieneone-thiophene D–A copolymers from our previous work.[26] In the case of some D–A copolymers such as poly(2,7-carbazole-altdithienylbenzothiadiazole) (PCDTBT),[27] it has been reported that the high-energy excitation generate more carrier than low energy pump. More detailed studies are currently underway to explore the interpretation.

The photoexcitation of PDTDPP-*alt*-BTZ thin film was investigated by transient photoinduced absorption spectroscopy in
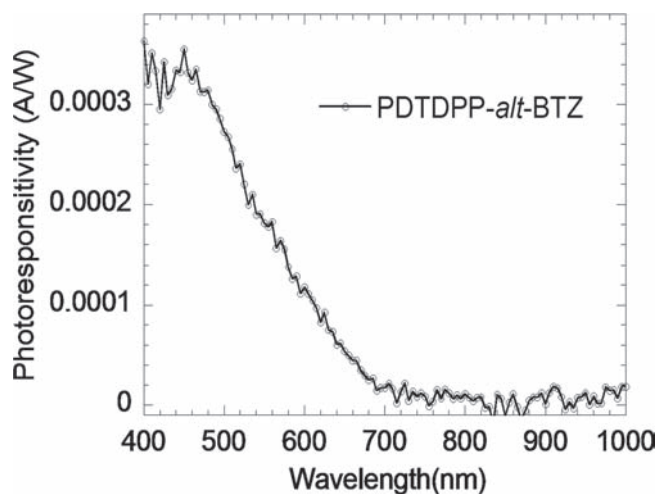

Figure 6. Photocurrent measurement of PDTDPP-*alt*-BTZ.

**ADVANCED
FUNCTIONAL
MATERIALS**
www.afm-journal.de
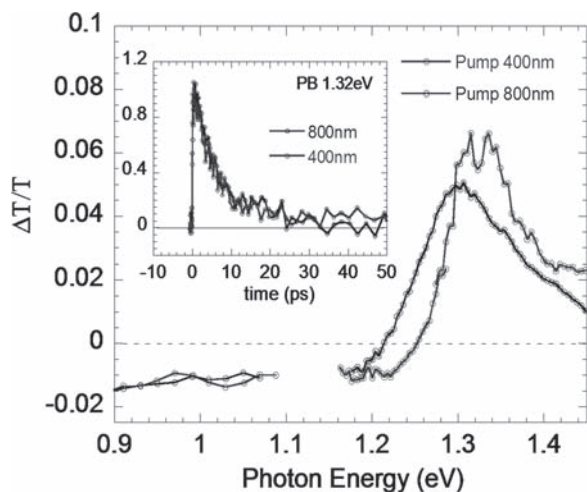
FULL PAPER

*Materials
Views*
www.MaterialsViews.com

Figure 7. Transient photoinduced absorption spectra of PDTDPP-*alt*-BTZ.

the visible and near infrared spectral ranges using excitation at 800 nm and 400 nm. The transient absorption spectra (TA) recorded at 0.5 ps time delay are shown in **Figure 7**. For 400 nm excitation, TA spectra show a broad negative photoinduced absorption band (PA) and a positive signal above 1.25 eV resulting from photo-bleaching (PB) of the absorption band of the pristine polymer. The TA spectra at 800 nm excitation shows a clear red shift compared to that for 400 nm excitation. The positive signal around 1.23 eV (the spectral range of the PL) was assigned to stimulated emission (SE) band for 800 nm pump. The absence of SE band for high energy pump (400 nm) shows the lower exciton generation efficiency, or possibly higher charge carrier yield, which has been observed in other D–A copolymers like PCDTBT. The inset shows the dynamics of photobleaching (PB) band for both pump wavelengths. The decay of the PB signal measures the recombination decay dynamics of all the photo-generated excitations. For PDTDPP-*alt*-BTZ thin film, the recombination is very fast with a lifetime of about 7 ps for both excitation wavelengths. The time decay for photoinduced absorption (PA) below 1.1 eV shows similar decay rate as that of PB. Since the photoconductivity is proportional to the lifetime of the carrier, the fast recombination of PDTDPP-*alt*-BTZ may one of the reasons for the low photocurrent.

3. Conclusion

In conclusion, we have demonstrated n-type, p-type equivalent ambipolar properties from the D–A conjugated copolymer, PDTDPP-*alt*-BTZ containing benzothiadiazole (BTZ), diketo-pyrrolopyrrole (DPP) and two unsubstituted thiophenes. DFT calculation results shows that the electron density of HOMO and LUMO are delocalized over the entire conjugated monomer (both the acceptor unit and donor unit). Ambipolar PDTDPP-*alt*-BTZ FETs show beautiful symmetry between p-type operation and n-type operation. The mobilities obtained from fully optimized FET with two color electrodes (Au for source electrode and Al for drain electrode)

were 0.1 cm^2 V^{-1} s^{-1} for the hole and 0.09 cm^2 V^{-1} s^{-1} for the electron. These values are among the highest reported for single-component polymer ambipolar transistors. The inverter constructed with the combination of two identical PDTDPP-*alt*-BTZ FETs exhibits a gain of ~35.

4. Experimental Section

FETs Fabrication: All FETs were fabricated on heavily n-type doped silicon (Si) wafers with a 200 nm thick thermally grown SiO$_2$ layer as shown in Figure S1. FETs were fabricated in the top contact geometry. The n-type doped Si substrate functioned as the gate electrode and the SiO$_2$ layer functioned as the gate dielectric. The semiconducting PDTDPP-*alt*-BTZ layer was spin-cast from solution at 3000 rpm. PDTDPP-*alt*-BTZ solution was prepared at 5 mg mL^{-1} concentration in chlorobenzene. The thickness of the PDTDPP-*alt*-BTZ films was approximately 60 nm. Prior to deposition of PDTDPP-*alt*-BTZ, the SiO$_2$ surface was modified with polypropylene-co-1-butene (PPcB) to remove hydroxyl groups from the SiO$_2$ surface. After PDTDPP-*alt*-BTZ deposition, the films were dried on hot plate stabilized at 80 °C for 30 min. The PDTDPP-*alt*-BTZ deposition was carried out in a controlled atmosphere glove box filled with N$_2$. Source and drain electrodes were deposited by thermal evaporation using a shadow mask. The thickness of source and drain electrodes was 50 nm. Channel length (*L*) and channel width (*W*) were 50 μm and 2.0 mm, respectively. Electrical characterization was performed under N$_2$ atmosphere using a Keithley semiconductor parametric analyzer (Keithley 4200).

Fabrication of PPcB Layer: The PPcB solution was prepared at 5 mg mL^{-1} concentration in Decahydronaphthalene, anhydrous solvent (Aldrich #294772). To completely dissolve, the PPcB solution was kept at 200 °C for 1 h. The PPcB layer was spin-cast from warm solution at 5000 rpm in air. After deposition, the samples were dried on hot plate stabilized at 200 °C for 20 min in air. Subsequently, the samples were moved to glove box filled with N$_2$ to deposit PDTDPP-*alt*-BTZ layer.

DFT Calculation: DFT calculations were performed using the Gaussian 03 package with the nonlocal hybrid Becke three-parameter Lee–Yang–Parr (B3LYP) function and the 6 –31G* basis set to elucidate the HOMO and LUMO levels after optimizing the geometry of PDTDPP-*alt*-BTZ using the same method.

UPS Measurement: The polymer solution was prepared in (chlorobenzene) with 5 mg mL^{-1} for PDTDPP-*alt*-BTZ. A gold film 75 nm thick was deposited on a pre-cleaned Si substrate with a thin native oxide. The PDTDPP-*alt*-BTZ solution was spin-coated at 2000 rpm on a gold film. Film fabrication was done in a N$_2$-atmosphere globe box. To minimize possible influence by exposure to air, the film was then transferred from the N$_2$-atmosphere dry box to the analysis chamber inside an air-free holder. Subsequently, the sample was kept inside a high-vacuum chamber overnight. The UPS analysis chamber was equipped with a hemispherical electron-energy analyzer (Kratos Ultra Spectrometer), and was maintained at 1.0 × 10^{-9} Torr. The UPS measurements were carried out using the He I (*hν* = 21.2 eV) source. The electron energy analyzer was operated at constant pass energy of 10 eV. During UPS measurements, a sample bias of –9 V was used in order to separate the sample and the secondary edge for the analyzer.

Transient Photoinduced Absorption Spectra (TA): The TA spectra was measured using pulsed laser pump/probe spectroscopy; the Ti:sapphire laser system with a regenerative amplifier that provides 100 fs pulses at photon energies of 1.55 eV, with 1 mJ per pulse at a repetition rate of 1 kHz. The pump beam was generated using either the fundamental emission from the Ti:sapphire laser at 800 nm or the second harmonic at 400 nm. The probe beam in the visible and near infrared spectral range was obtained from a white light supercontinuum and signal beam from optical parametric amplifier.

Materials and Instruments: All starting materials were purchased either from Aldrich or Acros and used without further purification. All solvents are ACS grade unless otherwise noted. Anhydrous THF was obtained by distillation from sodium/benzophenone prior to use. Anhydrous

www.MaterialsViews.com

ADVANCED
FUNCTIONAL
MATERIALS
www.afm-journal.de

FULL PAPER

toluene was used as received. 3,6-dithiene-2-yl-2,5-dihydropyrrolo[3,4-*c*]pyrrole-1,4-dione (DTDPP) and 2-decyltetradecylbromide were prepared according to established literature procedures. 4,7-Diboronicester-2,1,3-benzothiadiazole (BTZ) was purchased from Sigma-Aldrich Chemical Co., and subsequently recrystallized from methanol. ^{1}H NMR and ^{13}C NMR spectra were recorded on a VNMRS 600 (Varian, USA) spectrophotometer using CDCl$_3$ as solvent and tetramethylsilane (TMS) as the internal standard, and MALDI MS spectra were obtained from Ultraflex III (Bruker, Germany). UV–vis–NIR spectra were taken on Cary 5000 (Varian USA) spectrophotometer. Number-average (M_n) and weight average (M_w) molecular weights, and polydispersity index (PDI) of the polymer products were determined by gel permeation chromatography (GPC) with Agilent 1200 HPLC Chemstation using a series of mono disperse polystyrene as standards in THF (HPLC grade) at 308 K.

Synthesis of 3,6-dithiene-2-yl-2,5-di(2-decyltetradecyl)-pyrrolo[3,4-c]pyrrole-1,4-dione (1): A solution of 2-decyl-tetradecylbromide (9.1 g, 21.7 mmol) in anhydrous DMF (20 mL) was added dropwise to a mixture of 3,6-dithiene-2-yl-2,5-dihydropyrrolo[3,4-*c*]pyrrole-1,4-dione (2.8 g, 9.42 mmol), K$_2$CO$_3$ (3.0 g, 21.6 mmol) in anhydrous DMF (55 mL). The mixture was maintained at 120 °C overnight. The reaction was cooled to room temperature and poured into water (100 mL). The compound was extracted in CHCl$_3$, washed with brine, dried over MgSO$_4$. The solvent was evaporated under reduced pressure. The crude product was purified by chromatography on silica with 0–30% dichloromethane in hexane as eluent. Isolated yield = 5.1 g (55%) as a thick viscous dark purplish oil. ^{1}H NMR (CDCl$_3$, 600 MHz): δ ppm 8.88 (d, *J* = 3.85, 2H), 7.62 (d, *J* = 4.9, 2H), 7.27 (d, *J* = 8.89, 2H), 4.03 (d, *J* = 7.71, 4H), 1.91 (m, 2H), 1.30–1.21 (m, 80H), 0.89–0.87 (m, 12H). ^{13}C NMR (CDCl$_3$, 150 MHz): δ ppm 161.75, 140.43, 135.19, 130.44, 129.84, 120.38, 107.95, 46.23, 37.75, 31.93, 29.69, 29.67, 29.65, 29.38, 29.37, 29.36, 26.22, 22.70, 22.69, 14.13. MALDI-TOF MS (*m/z*) 973.59(M$^+$). Anal. Calcd for C$_{62}$H$_{104}$N$_2$O$_2$S$_2$: C, 76.48; H,10.77, N, 2.88. Found: C, 77.04; H, 10.97, N, 2.96.

Synthesis of 3,6-Di(2-bromothien-5-yl)-2,5-di (2-decyltetradecyl)-pyrrolo[3,4-c]pyrrole-1,4-dione (2): N-Bromosuccinimide (NBS, 1.26 g, 7.08 mmol) was added slowly to a solution of **1** (3 g, 3.08 mmol) in CHCl$_3$ (100 mL). The solution was protected from light and stirred at room temperature for 48 h. The reaction mixture was poured into water (100 mL) and extracted in CHCl$_3$. The organic layer was dried over MgSO$_4$ and the solvent was evaporated under reduced pressure. The crude product was purified by chromatography on silica with 0–50% dichloromethane in hexane as eluent. Isolated yield = 1.8 g (53%) as a thick viscous dark purplish oil. ^{1}H NMR(CDCl$_3$, 600 MHz): δ ppm 8.62 (d, *J* = 4.18, 2H), 7.21 (d, *J* = 4.17, 2H), 3.91 (d, *J* = 7.71, 4H), 1.87 (m, 2H), 1.29–1.21 (m, 80H), 0.89–0.86 (m, 12H). ^{13}C NMR (CDCl$_3$, 150 MHz): δ ppm 161.61, 139.39, 135.31, 131.42, 131.17, 118.95, 108.01, 46.36, 37.77, 31.94, 30.00, 29.70, 29.68, 29.66, 29.57, 29.39, 26.20, 22.70, 14.13. MALDI–TOF MS(m/z) 1131.45(M$^+$). Anal. Calcd for C$_{62}$H$_{102}$Br$_2$N$_2$O$_2$S$_2$: C, 65.82; H, 9.09 N, 2.48. Found: C, 68.14; H, 9.36, N, 2.43.

Synthesis of Poly[3,6-dithiene-2-yl-2,5-di(2-decyltetradecyl)-pyrrolo[3,4-c]pyrrole-1,4-dione-5′,5″-diyl-alt-benzo-2,1,3-thiadiazol-4,7-diyl] (PDTDPP-alt-BTZ): 2,1,3-Benzothiadiazole-4,7-bis(boronic acid pinacol ester) (67 mg, 0.17 mmol), dibromide **2** (200 mg, 0.17 mmol), Aliquat 336 (8 mg, 13 mol%), 2 M aqueous K$_2$CO$_3$ (7 mL), and toluene (10 mL) were placed together in a Schlenk flask and purged with argon for 15 min. To this solution, tetrakis(triphenylphosphine)palladium (10 mg g, 8.6 μmol) was added and the reaction mixture was heated at 95 °C under vigorous stirring for 72 h. The reaction was poured into a mixture of methanol and 2.0 M HCl (1:1, 300 mL) and filtered. The collected dark solid was redissolved in chlorobenzene (10 mL) and added dropwise to methanol (200 mL). The resulting solid was filtered off and subjected to sequential Soxhlet extraction with methanol (1 d), acetone (1 d), and hexane (1 d) to remove low molecular weight fraction of the materials. The residue was extracted with chlorobenzene to give dark purplish product after precipitating again from methanol and drying in vacuo. Isolated yield of polymer PDTDPP-*alt*-BTZ = 150 mg (75%). GPC analysis M_n = 135.6 kg mol^{-1}, M_w = 595 kg mol^{-1}, and PDI = 4.26 (against PS standard). ^{1}H NMR (CDCl$_3$, 600 MHz): δ ppm 9.13–9.09 (br, 2H), 8.24–8.16

(br, 2H), 8.08–7.96 (br, 2H), 4.23–4.06 (br, 4H), 2.32–2.29 (t, 2H), 1.34–1.03 (br, 80H), 0.90–0.85 (br, 12H). Anal. Calcd for C$_{68}$H$_{105}$BrN$_4$O$_2$S$_3$: C, 68.82; H, 8.92 N, 4.72 Found: C, 68.61; H, 9.19, N, 5.61.

[1] Z. Bao, J. Locklin, in *Organic Field-Effect Transistors*, CRC Press, Boca Raton, FL **2007**.

[2] E. J. Meijer, D. M. De Leeuw, S. Setayesh, E. Van Veenendaal, B. H. Huisman, P. W. M. Blom, J. C. Hummelen, U. Scherf, T. M. Klapwijk, *Nat. Mater.* **2003**, *2*, 678.

[3] B. Crone, A. Dodabalapur, Y. Y. Lin, R. W. Filas, Z. Bao, A. LaDuca, R. Sarpeshkar, H. E. Katz, W. Li, *Nature* **2000**, *403*, 521.

[4] L. Bürgi, M. Turbiez, R. Pfeiffer, F. Bienewald, H. J. Kirner, C. Winnewisser, *Adv. Mater.* **2008**, *20*, 2217.

[5] I. McCulloch, M. Heeney, C. Bailey, K. Genevicius, I. Macdonald, M. Shkunov, D. Sparrowe, S. Tierney, R. Wagner, W. M. Zhang, M. L. Chabinyc, R. J. Kline, M. D. McGehee, M. F. Toney, *Nat. Mater.* **2006**, *5*, 328.

[6] H. Sirringhaus, P. J. Brown, R. H. Friend, M. M. Nielsen, K. Bechgaard, B. M. W. Langeveld-Voss, A. J. H. Spiering, R. A. J. Janssen, E. W. Meijer, P. Herwig, D. M. de Leeuw, *Nature* **1999**, *401*, 685.

[7] J. C. Bijleveld, A. P. Zoombelt, S. G. J. Mathijssen, M. M. Wienk, M. Turbiez, D. M. de Leeuw, R. A. J. Janssen, *J. Am. Chem. Soc.* **2009**, *131*, 16616.

[8] N. Blouin, A. Michaud, D. Gendron, S. Wakim, E. Blair, R. Neagu-Plesu, M. Belletete, G. Durocher, Y. Tao, M. Leclerc, *J. Am. Chem. Soc.* **2008**, *130*, 732.

[9] A. P. Zoombelt, S. G. J. Mathijssen, M. G. R. Turbiez, M. M. Wienk, R. A. J. Janssen, *J. Mater. Chem.* **2010**, *20*, 2240.

[10] H. Usta, A. Facchetti, T. J. Marks, *J. Am. Chem. Soc.* **2008**, *130*, 8580.

[11] P. Sonar, S. P. Singh, Y. Li, M. S. Soh, A. Dodabalapur, *Adv. Mater.* **2010**, *22*, 5409.

[12] E. J. Zhou, S. P. Yamakawa, K. Tajima, C. H. Yang, K. Hashimoto, *Chem. Mater.* **2009**, *21*, 4055.

[13] M. Kastler, W. Pisula, D. Wasserfallen, T. Pakula, K. Müllen, *J. Am. Chem. Soc.* **2005**, *127*, 4286.

[14] O. Wallquist, R. Lenz, *Macromol. Symp.* **2002**, *187*, 617.

[15] J. H. Seo, R. Q. Yang, J. Z. Brzezinski, B. Walker, G. C. Bazan, T. Q. Nguyen, *Adv. Mater.* **2009**, *21*, 1006.

[16] S. Braun, W. R. Salaneck, M. Fahlman, *Adv. Mater.* **2009**, *21*, 1450.

[17] H. Ishii, K. Sugiyama, E. Ito, K. Seki, *Adv. Mater.* **1999**, *11*, 605.

[18] Y. L. Gao, *Acc. Chem. Res.* **1999**, *32*, 247.

[19] J. Hwang, A. Wan, A. Kahn, *Mater. Sci. Engineer.* **2009**, *R 64*, 1.

FULL PAPER

[20] L. L. Chua, J. Zaumseil, J. F. Chang, E. C. W. Ou, P. K. H. Ho, H. Sirringhaus, R. H. Friend, *Nature* **2005**, *434*, 194.

[21] S. Cho, J. H. Seo, K. Lee, A. J. Heeger, *Adv. Funct. Mater.* **2009**, *19*, 1459.

[22] S. J. Mun, K. Lee, K. H. Lee, M. S. Oh, S. Im, *Org. Electron.* **2010**, *11*, 169.

[23] E. Cantatore, T. C. T. Geuns, G. H. Gelinck, E. van Veenendaal, A. F. A. Gruijthuijsen, L. Schrijnemakers, S. Drews, D. M. de Leeuw, *IEEE J. Solid-State Circuits* **2007**, *42*, 84.

[24] C. A. Di, G. Yu, Y. Q. Liu, X. J. Xu, D. C. Wei, Y. B. Song, Y. M. Sun, Y. Wang, D. B. Zhu, J. Liu, X. Y. Liu, D. X. Wu, *J. Am. Chem. Soc.* **2006**, *128*, 16418.

[25] S. Cho, J. H. Seo, S. H. Kim, S. Song, Y. Jin, K. Lee, H. Suh, A. J. Heeger, *Appl. Phy. Lett.* **2008**, *93*, 263301.

[26] C. Yang, S. Cho, R. C. Chiechi, W. Walker, N. E. Coates, D. Moses, A. J. Heeger, F. Wudl, *J. Am. Chem. Soc.* **2008**, *130*, 16524.

[27] S. H. Park, A. Roy, S. Beaupre, S. Cho, N. Coates, J. S. Moon, D. Moses, M. Leclerc, K. Lee, A. J. Heeger, *Nat. Photonics* **2009**, *3*, 297.